Acta Mech
https://doi.org/10.1007/s00707-026-04813-3

ORIGINAL PAPER

Rodrigo Martín-Sáiz · Blas Herrera

Design of bending-moment-free catenary arches of finite thickness: a discrete geometric approach

Received: 17 March 2026 / Revised: 15 June 2026 / Accepted: 18 June 2026

Abstract Although a one-dimensional catenary arch subjected to its self-weight is simply compressed and bending-moment-free, when this arch is three-dimensional and has a constant rectangular cross-section of finite dimensions, the centroids of its voussoirs are displaced towards the extrados. This displacement prevents the arch from being geometrically compatible with a bending-moment-free state, a contradiction known as the catenary arch bending-moment-free paradox [1]. Firstly, this paper demonstrates that this paradox is not exclusive to rectangular cross-sections, but extends to any trapezoidal cross-section, ruling out any continuous solution to the centroid eccentricity problem. This impossibility result motivates a discrete approach to solve a geometrical problem: find the voussoir geometry such that the eccentricity between the centroidal axis and the catenary curve is zero for all voussoirs, subject to the constraint of uniform volume distribution along the catenary axis. The proposed method is based on the discretisation of a catenary curve into small segments of equal length, such that both the volumetric centroids of the voussoirs and the centroids of the normal sections are located on the catenary curve. Three alternative designs for the voussoir shape are developed and analysed. The method is founded on a closed-form analytical geometric formulation, and the accuracy of the solution increases with the number of voussoirs. Furthermore, a closed-form expression for the minimum number of voussoirs required to achieve a prescribed accuracy is derived. The outcomes obtained from the design of various arches reveal the geometric and structural properties of the resulting forms. The proposed design has been verified by graphic statics, confirming that the resulting arches are geometrically compatible with a bending-moment-free state. The described method could be part of an integrated process of designing and manufacturing voussoirs using 3D printing for more efficient arches and vaulted structures.

1 Introduction

1.1 Catenary as the perfect arch

According to the principle of inversion formulated by Robert Hooke in 1675 [2], a catenary arch should be simply compressed and bending-moment-free, just as its inverse form, a hanging chain, is simply tensioned and bending-moment-free. A chain can be regarded as a one-dimensional element because the dimensions of its cross-section can be neglected, being negligible compared to its length. Consequently, a hanging chain forms a curved axis along which its self-weight is evenly distributed. This curved axis is a simply tensioned

R. Martín-Sáiz (✉)
Department of Architectural Technology, Universitat Politècnica de Catalunya – Barcelona Tech (UPC), Av. Diagonal 649, 08028 Barcelona, Spain
e-mail: rodrigo.martin@upc.edu

B. Herrera
Department of Computing Engineering and Mathematics, Universitat Rovira i Virgili, Av. Paisos Catalans 26, 40307 Tarragona, Spain

Published online: 22 July 2026

funicular polygon comprising infinitesimally small segments, and the shape of this curved axis is referred to as a catenary curve. The mathematical description of this curve was formulated in 1691 by Gottfried W. Leibniz [3], Christiaan Huygens [4] and Johan Bernoulli [5] as a solution to the problem posed by the latter's brother Jakob Bernoulli [6]. Subsequently, in 1697, David Gregory affirmed that, in addition to the catenary curve representing the most perfect form of a one-dimensional arch (i.e., an arch of infinitesimal thickness), any stable three-dimensional arch (i.e., an arch of finite thickness), regardless of its shape, must be capable of inscribing a catenary curve within itself [7]. In 1717, James Stirling formulated a method for the arrangement of spheres along an axis with the shape of an inverted chain [8]. In 1748, Giovanni Poleni used chains with spheres of several diameters, equivalent to the self-weight distribution in his analysis of the St. Peter's dome in Rome [9]. Both authors proposed a solution to the problem of the catenary arch by means of a discrete approximation based on the equilibrium of "spherical voussoirs". This is known as Stirling-Poleni's model. All of these discoveries initiated a revolution in the understanding of arch mechanics.

1.2 The shape of the thrust line and the problem of inversion: from one-dimensional arch to three-dimensional arch

Since David Gregory's statement [7], the equivalence between the catenary curve and the shape of the thrust line for any arch shape was historically assumed [10, 11], but, recently, this statement has been demonstrated to be not completely true for any arch shape [12–14]. Only if the centroidal axis of the arch is a catenary curve, can the shape of a thrust line coincide with a catenary curve [15]. In addition, if the finite dimensions of the cross-section are neglected, many authors consider that the catenary arch is simply compressed and free of bending moments [16–18].

Catenary arches are commonly defined by a catenary curve from which the extrados and the intrados are equidistant. Thus, the catenary curve and the mid-axis line are coincident. However, approximately a century after the formulation of the inversion principle, Leonardo Salimbeni demonstrated the disparity between the mid-axis line of a catenary arch of finite thickness, characterised by equidistant extrados and intrados, and the axis joining the centroids of the arch's voussoirs [19]. Centuries later, Milutin Milanković revisited this problem to formulate his theory about the thrust line in arches [20]. Milanković devised a mathematical apparatus he termed the infinitesimal voussoir [21]. It can be defined as the volumetric region of arch between two normal sections which are so close that the value of the angle between them is confounded with the value of the sine of the same angle. The centroid of this voussoir is not located at a point equidistant from the extrados and the intrados, but is instead displaced slightly towards the extrados. This displacement η is contingent on the curvature $1/R$ of the arch, according to Eq. (1). It is evident that as the curvature of the arch increases, the displacement of the centroid of the infinitesimal voussoir towards the extrados of the arch also increases. The geometric location of the centroids of the infinitesimal voussoirs is termed the centroidal axis of the three-dimensional arch, i.e., the centroidal axis of the catenary arch of finite thickness.

$$\eta = \frac{t^2}{12R} \tag{1}$$

Recent studies [1, 22–24] have revisited this problem, utilising the concept of the infinitesimal voussoir to demonstrate that the centroidal axis of a three-dimensional catenary arch formed by the extrusion of a rectangular section along a catenary curve does not coincide with the catenary curve itself. Instead, it is found to be displaced towards the extrados of the arch. This displacement is at its maximum at the keystone of the arch, where the curvature is also maximum, and decreases progressively as we move away from this point. Consequently, as evidenced by the works of Nikolić [1, 22], this discrepancy hinders the capacity of a catenary arch of rectangular section to be completely free of bending moments. This is due to the inability to locate a thrust line passing through the centroids of all the arch's normal sections, where each centroid is situated at the centroid of each section. This issue has been termed by Nikolić "the catenary arch bending-moment-free paradox" [1] and highlights the complexity of equating, through inversion, the mechanical behaviour of a one-dimensional element (i.e., an element of infinitesimal thickness, such as a hanging chain) to the behaviour of a three-dimensional element (such as a catenary arch, which is defined by the non-infinitesimal dimensions of its normal cross-section), despite both elements having the same longitudinal shape. This is further substantiated by the findings of Alexakis and Makris [25].

As Nikolić demonstrated, taking into account all possible thrust lines inscribed in a catenary arch of constant thickness, there is one that passes through the centroids of all of the voussoirs. This is the thrust line closest to the catenary curve, which joins the centroids of the normal sections, rather than coinciding with the mid-axis line. Then, the eccentricity of the voussoir's centroids with respect to the catenary curve is equal to the distance of the closest thrust line and the catenary curve passing through the centroids of the normal cross-sections [1]. This can also be demonstrated by using graphic statics, as shown in subSect. 2.3 of this article. This impossibility of achieving a bending-moment-free state in a continuous sense for a catenary arch of finite thickness with constant rectangular cross-section motivates the search for an alternative design approach.

1.3 Conditions for the design of a three-dimensional catenary arch geometrically compatible with a bending-moment-free state

This paper presents a discrete method to solve this paradox, formulated as a geometric problem subject to two conditions: (1) the volume of all voussoirs remains constant, and (2) the eccentricity between the centroidal axis and the catenary curve is zero for all voussoirs. To this end, a three-dimensional catenary arch is designed whose volume is uniformly distributed along a catenary axis containing both the centroids of the voussoirs and the centroids of the arch's normal cross-sections. The first condition is intrinsic to the definition of a catenary arch, which supports only its self-weight uniformly distributed along its length. Both conditions imply the existence of a thrust line coinciding with the shape of the catenary curve. The absence of eccentricity between this thrust line and the centroid of any of the arch's normal cross-sections makes the arch geometrically compatible with a bending-moment-free state. The accuracy of the solution increases with the number of voussoirs n. This issue is addressed at the end of Sect. 3.

1.4 Theoretical framework and objective

The method described in this paper is carried out within a geometric framework in which voussoirs are considered rigid blocks, joints are assumed to have no tensile strength and the stress flow is conducted through the contact faces between voussoirs, in analogy with the Stirling-Poleni model of spherical voussoirs [8, 9], and structural stability is evaluated based on the position of the thrust line with respect to the axis and the limits of the arch [26–31]. This framework remains the most widely accepted approach for the analysis and design of voussoir arches [12–14, 22–25], and is currently fully relevant thanks to the development of computational tools [32–34], many of which are rooted in graphic statics given its ability to simultaneously determine funicular forms corresponding to thrust lines and quantify the forces they represent [35–38].

Taking into account this framework, the objective of the proposed method is to find a design of the voussoirs of the catenary arch geometrically compatible with the existence of a thrust line passing through the centroids of the normal cross-sections, describing a catenary curve and thus geometrically compatible with a bending-moment-free state. According to the safe theorem formulated by Kooharian [26] and Heyman [27, 28], the existence of a thrust line contained within the profile of the arch is a sufficient condition to guarantee its stability, without the need to know the real stress state. The geometrical factor of safety, defined as the ratio between the real thickness of the arch and the minimum thickness capable of containing a single thrust line, tends to infinity for any catenary arch under self-weight [27, 28], since the eccentricity η decreases with the arch thickness [1, 22], making this factor impractical for comparing different catenary arch designs. Tempesta and Galassi [39–41] addressed this limitation through a performance factor $k = (t - 2\eta)/t$, with $0 \leq k \leq 1$, which reaches its maximum value $k = 1$ only when $\eta = 0$, corresponding to the widest possible domain of admissible thrust lines and therefore to the greatest safety margin against any additional load. In the present paper, graphic statics has been used to verify the existence of such a thrust line in the designs obtained by the proposed method, as it constitutes a rigorous and widely used verification tool, fully consistent with the geometric and discrete approach of this work and with the discrete nature of voussoir arches [35, 36].

2 Method

2.1 Definition of the catenary curve describing the arch's axis

Let there be a catenary curve contained in a vertical plane *XZ*, for which a system of variable Cartesian coordinates (x, y, z) have been considered in the three-dimensional affine space. The catenary curve under consideration has a maximum height H and a span L, both of which are known (cf. Fig. 2a). The ends of the

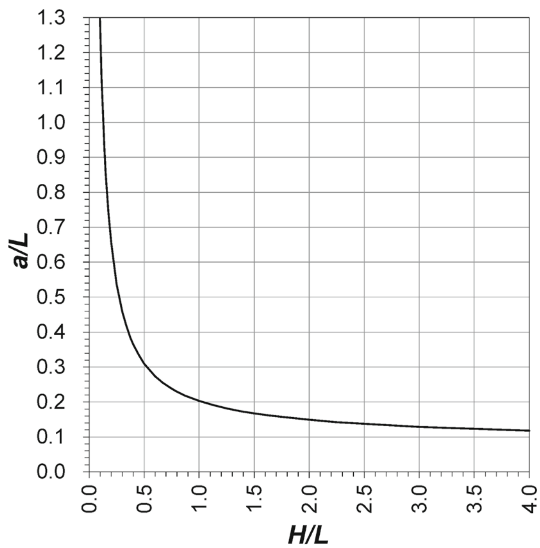

Fig. 1 Variation of the ratio a/L of the catenary curve as a function of the arch's H/L ratio

curve are located on the X-coordinate axis, while its vertex is situated on the Z-coordinate axis. The catenary curve is defined by Eq. (2). If the coordinates of the three known points ($-L/2$,0), (0,H) and ($L/2$,0), expressed in Cartesian coordinates (x, z), are substituted in Eq. (2), Eqs. (3) and (4) can be derived. Therefore, a system of two equations, (2) and (3), and two unknowns (a and c) is obtained. The Newton–Raphson iterative method is then applied to Eq. (4) to solve the system.

$$z = \gamma(x) = a \cosh \frac{x}{a} + c \tag{2}$$

$$c = H - a \tag{3}$$

$$a \cosh\left(\frac{L}{2a}\right) + H - a = 0 \tag{4}$$

Figure 1 shows the variation of the ratio a/L of the catenary curve as a function of the arch's H/L ratio. The ratios a/L were obtained by means of the procedure described in the previous paragraph. This graphic provides an easy way to know the parameters of the catenary curves for arches with $0.1 \leq H/L \leq 4.0$.

2.2 Defining the shape of the voussoirs in the plane of the arch

The length s of the catenary curve, measured from the vertex in the positive direction of the x-coordinate, is defined by Eq. (5), and the radius of curvature R of this curve, as a function of this parameter s, is determined by Eq. (6).

$$s(x) = a \sinh \frac{x}{a} \tag{5}$$

$$R(s) = \frac{s^2 + a^2}{|a|} \tag{6}$$

Knowing this, the catenary curve is discretised into n equal segments of length ε such that $n >> 1$. This expression signifies that the number n should be sufficiently large, and consequently a length ε should be sufficiently small, so that discretisation inaccuracies are negligible compared to the desired final accuracy. This issue is addressed at the end of Sect. 3.

Next, for each curve segment, each voussoir is modelled as an isosceles trapezium of height t in the plane of the arch, where t is uniform across all the voussoirs (see Fig. 2b). This approximation of the voussoir's shape to an isosceles trapezium has antecedents in the work of Milanković [20], and Nikolić [1, 22] and Tempesta

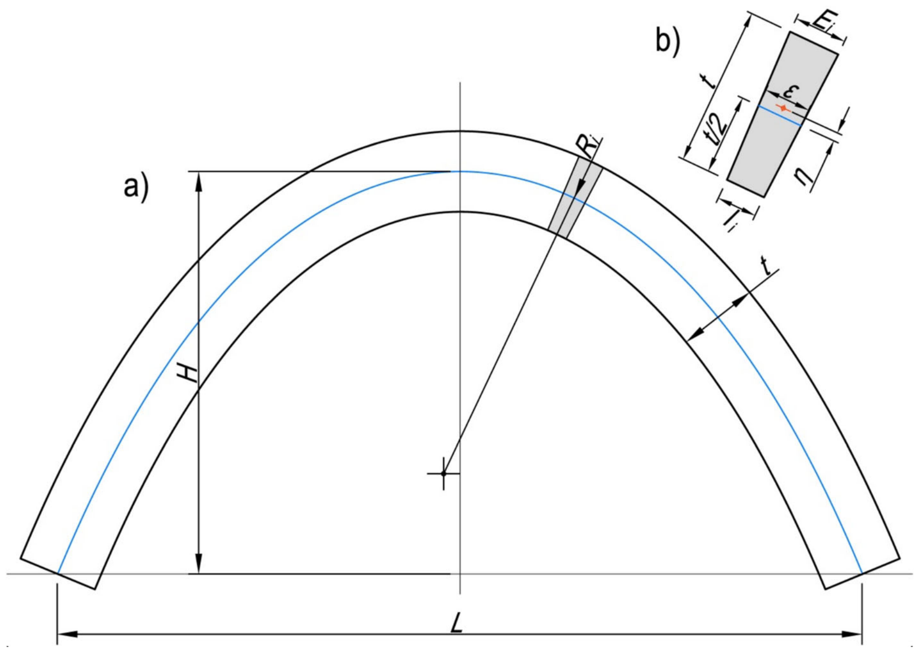

Fig. 2 Parameters for defining the shape of the arch (**a**); parameters for defining the shape of the voussoirs in the plane of the arch (**b**)

and Galassi [39]. The lengths of the bases of the trapezium forming each voussoir are designated E_i and I_i (i-th voussoir). These bases are situated on the extrados and intrados of the arch, respectively. It is assumed that the arch's mid-axis line (illustrated in blue in Fig. 2a, b), the points of which are equidistant from the extrados and the intrados) coincides with the catenary curve. The values of E_i and I_i are then determined by Eqs. (7) and (8), respectively,

$$E_i = \frac{\varepsilon\left(R_i + \frac{t}{2}\right)}{R_i} \tag{7}$$

$$I_i = \frac{\varepsilon\left(R_i - \frac{t}{2}\right)}{R_i} \tag{8}$$

where R_i denotes the radius of curvature of the catenary curve at the midpoint of each segment of length ε, calculated in accordance with Eq. (6).

2.3 The issue of the eccentricity of the voussoirs' centroids

If the trapezium is extruded to create a width b (which is constant along the entire length of the arch) in a direction perpendicular to the plane of the catenary curve, a straight trapezoidal prism is obtained whose volume is approximately equal to the volume of the real voussoir of the catenary arch with a constant rectangular normal cross-section. This prism has height t and width b. Clearly, the larger the value of n and, consequently, the smaller the value of ε, the better the approximation will be.

The eccentricity η of the centroid of the trapezoidal voussoir with respect to the centroid of the normal cross-section, as illustrated in Fig. 2b, is expressed in Eq. (9). If in Eq. (9) we substitute E and I with the expressions from Eqs. (6) and (7), the result is Eq. (1) derived by Milanković [1, 20, 22].

$$\eta_i = \frac{t}{2} - \frac{t(2I_i + E_i)}{3(I_i + E_i)} \tag{9}$$

This non-zero eccentricity η implies a disparity between the axis joining the centroids of the voussoirs and the axis joining the centroids of the arch's normal cross-sections (mid-axis line). As explained in sub-Sect. 1.2, the axis joining the centroids of the voussoirs coincides with the thrust line closest to the mid-axis line [1]. This

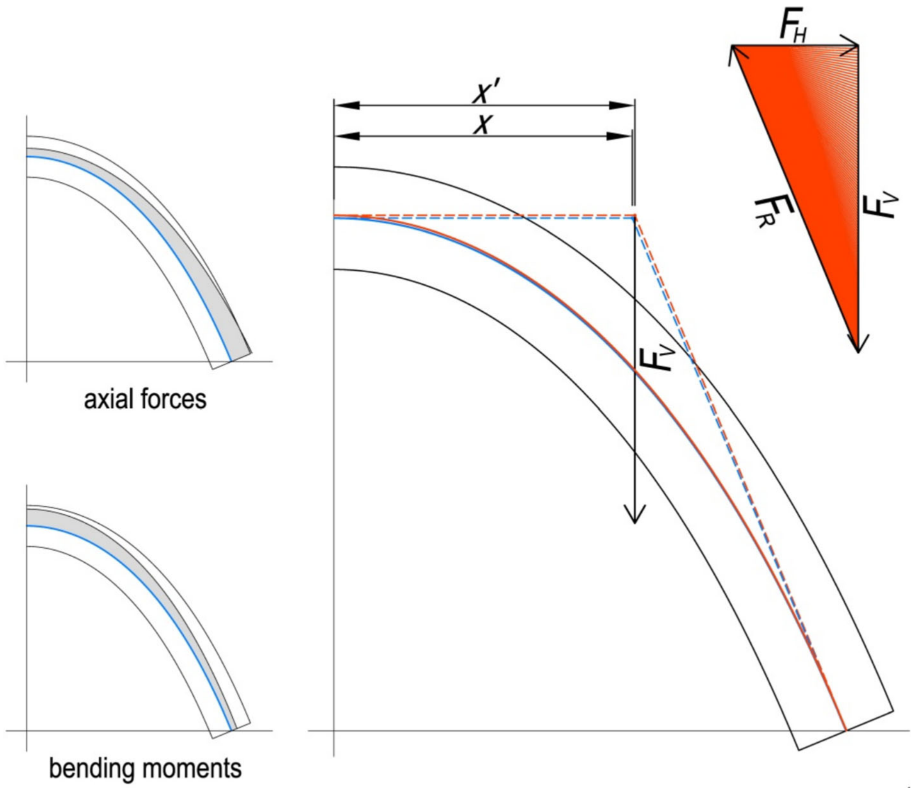

Fig. 3 Semi-catenary arch of constant thickness. In blue colour is represented the mid-axis line coinciding with the catenary, and in red colour the axis joining the real centroids of the voussoirs. If the volumetric centroids were erroneously assumed to coincide with the catenary, F_V would act at x; in reality [1, 22], F_V acts at $x' > x$, generating the bending moments shown on the left

can be demonstrated by using graphic statics, as shown in Fig. 3. If the volumetric centroids of the voussoirs are erroneously assumed to coincide with the catenary, the vertical component F_V of the resultant force at the springing would act at a horizontal distance x from the keystone, the thrust line would coincide with the mid-axis line, and the arch would be geometrically compatible with a bending-moment-free state. However, in reality [1, 22], the volumetric centroids are displaced towards the extrados, so that F_V acts at $x' > x$. If the resultant forces F_R and F_H, at the base and the keystone respectively, are aligned with the ends of the axis joining the real centroids of the voussoirs, the resulting funicular polygon (in red in Fig. 3), i.e., the thrust line closest to the mid-axis line coincides with the axis joining the real centroids of the voussoirs. The eccentricity η of this thrust line with respect to the mid-axis line causes a bending moment. The variation of this bending moment depends on the variation of the eccentricity and the axial force. The values of the bending moment in the diagram have been exaggerated to better appreciate them in the figure. Note that the axial force increases from the keystone to the base of the arch, while the eccentricity increases from the base to the keystone. As a result of these variations, the bending moments decrease slightly from the keystone to the base.

Figure 4 shows the elevation of six arches considering three catenary curves and two different arch thicknesses t. It is evident from the figure that the centroidal axis (in red) is displaced above the catenary curve (in blue) towards the extrados of the arch. This displacement, or eccentricity η, is maximum in the keystone of all arches and decreases progressively as the voussoirs are closer to the arch's springing, although it does not reach zero. Furthermore, it is evident that the magnitude of η increases with the ratio H/L of the arch and with the value of t.

To further elucidate the disparity between the centroids of the voussoirs and the catenary curve, Fig. 5a provides a visual representation of the performance factor $k = (t - 2\eta)/t$ [39–41] as a function of the ratio H/L, for six different slendernesses $\lambda = L/t$ of the arch's cross-section. In addition, Fig. 5b shows the variation of the ratio between the normal stress σ_M due to the bending moment and the normal stress σ_N due to the axial force in the keystone, depending on the ratio H/L and the slendernesses $\lambda = L/t$ of each arch. It should be noted that this ratio does not represent the real stress state of the arch, but rather the stress state

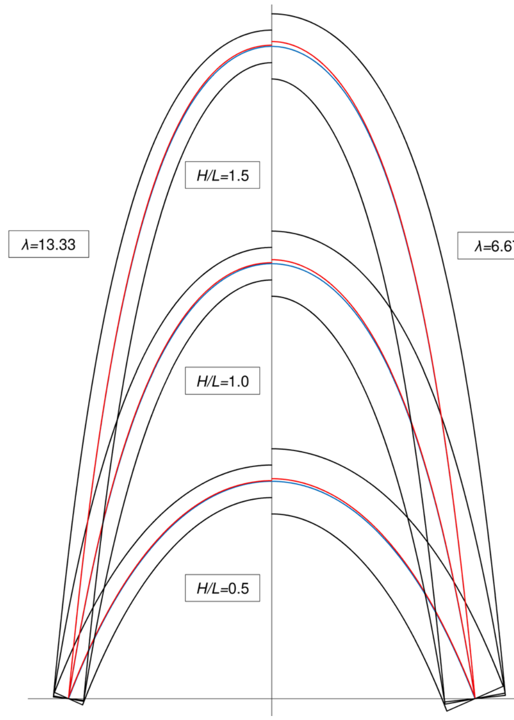

Fig. 4 Elevation of six arches with a constant rectangular normal cross-section, considering three catenary curves and two arch thicknesses t. The blue colour indicates the catenary curve where the centroids of the normal cross-sections are located, while the red colour represents the axis joining the centroids of the voussoirs

corresponding to the optimal equilibrium condition, i.e., that of the thrust line closest to the mid-axis line. This ratio is computed here for comparison purposes, as it will be used in Sect. 3 to demonstrate that, in catenary arches geometrically compatible with a bending-moment-free state, the increase in normal stress due to the weight of the additional prisms is smaller than the increase due to the bending moment in the optimal state of a conventional catenary arch.

It is evident from the graphs in Fig. 5 that the performance factor k and the normal stress σ_M approach their limit values, $k \to 1$ and $\sigma_M \to 0$, as the ratio H/L approaches zero; i.e., when the arch is so flat that its curvature is zero. Furthermore, it is observed that the greater the slenderness λ, the smaller normal stress σ_M and the closer k is to 1, but the more gradual the k variation as a function of the arch's H/L ratio. This indicates that the deviation of k from 1 and the normal stress σ_M due to the bending moment of an arch with ratio $H/L = 4$ and slenderness $\lambda = 8$ are almost five times greater than that of an arch with the same ratio and slenderness $\lambda = 40$.

2.4 On the impossibility of a continuous solution to the centroid eccentricity problem in voussoirs with the variation of trapezoidal cross-sections

Given a two-dimensional trapezoidal voussoir as shown in Fig. 2b, of height t, and bases E and I, located at the extrados and intrados of the arch respectively, Eq. (10) is used to calculate the width $l(z)$ of the trapezoid at height z, with $z = 0 \div t$, where z is the coordinate measured from the extrados in the perpendicular direction towards the intrados

$$l(z) = E - \frac{(E - I)}{t} z \tag{10}$$

In general terms, for a three-dimensional voussoir we can define $\eta = d_{E,S} - d_{E,V}$, where $d_{E,S}$ is the distance between the extrados and the centroid of the normal cross-section of the voussoir, and $d_{E,V}$ is the distance between the extrados and the centroid of the volume of the voussoir. This expression is developed in

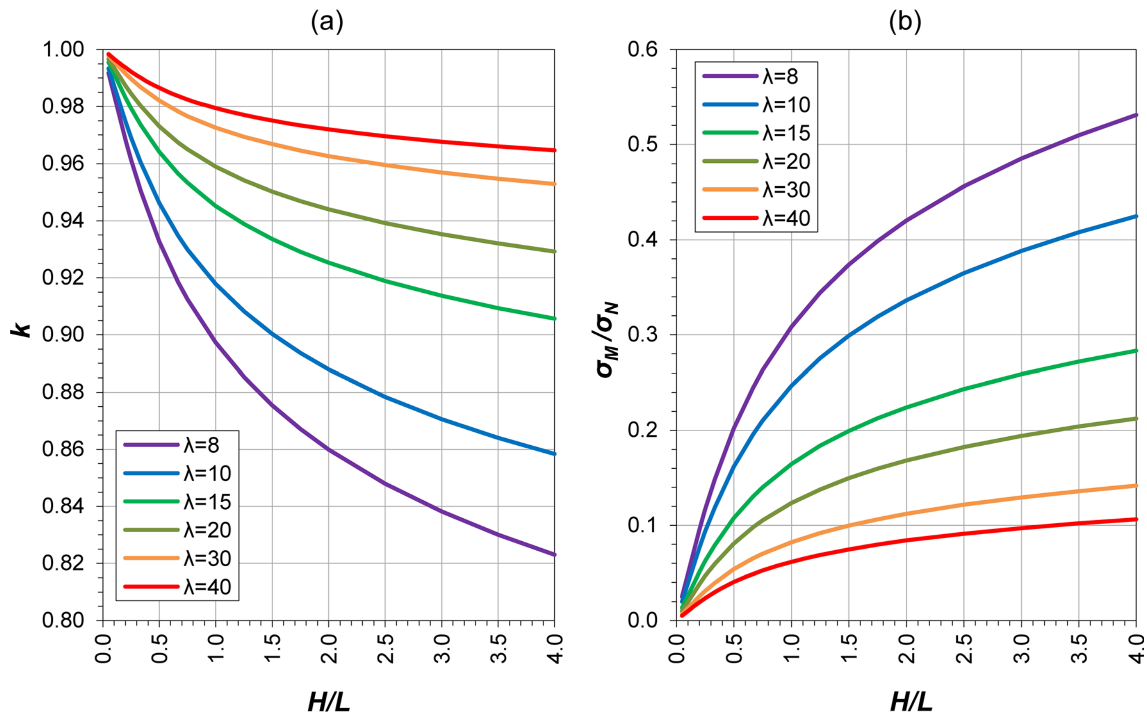

Fig. 5 Variation of the performance factor $k = (t - 2\eta)\big/t$ (**a**) and of the ratio $\sigma_M\big/\sigma_N$ (**b**), both as a function of the arch's $H\big/L$ ratio, for six distinct slendernesses $\lambda = L\big/t$

Eq. (11), in which $b(z)$ is the function defining the width of the normal cross-section. Note that Eq. (11) is a generalisation of Eq. (8) for any function $b(z) \geq 0$.

$$\eta = \frac{\int_0^t z \cdot b(z)\mathrm{d}z}{\int_0^t b(z)\mathrm{d}z} - \frac{\int_0^t z \cdot b(z) \cdot l(z)\mathrm{d}z}{\int_0^t b(z) \cdot l(z)\mathrm{d}z} \tag{11}$$

By extruding the trapezoidal shape of the two-dimensional voussoir of Fig. 2b by a width b in the direction perpendicular to the plane of the trapezoid, a three-dimensional voussoir is obtained whose normal cross-section is the rectangle b x t. Given that $b(z) = A\big/t$, the distance η between the centroid of the three-dimensional voussoir and the centroid of the rectangular normal section is identical to the distance η that would be obtained in the two-dimensional voussoir, η can be calculated by means of Eq. (1), formulated by Milanković [20].

Now, instead of $b(z) = b$, let us consider a second, slightly more complex three-dimensional voussoir, in which $b(z) = mz + n$ with the restriction $b(z) \geq 0$ and with $z = 0 \div t$. The normal section of this second voussoir would no longer be a rectangle, but an isosceles trapezoid of height t and variable width $b(z) = mz+n$, in which we will maintain the condition that $b\left(t\big/2\right) = A\big/t$ so that the area of this new normal section is identical to the area of the normal section of the three-dimensional voussoir with a rectangular normal section. We aim to demonstrate that, just as in a voussoir with a rectangular normal section, in a voussoir with a trapezoidal normal cross-section $\eta > 0$. All of these parameters are represented in Fig. 6.

The denominator of the first term of Eq. (11) is the area A of the normal section, that is $A = t\varepsilon$, and the denominator of the second term is the volume V of the three-dimensional voussoir, that is $V = t\varepsilon\overline{b}$, where $\varepsilon = \frac{E+I}{2}$ Therefore, in Eq. (11) all these terms are substituted in the denominators, and additionally $l(z)$ is substituted by the expression of Eq. (10) and $b(z)$ by the expression $mz + n$. This yields Eq. (12).

$$\frac{\int_o^t z(mz+n)\mathrm{d}z}{A} - \frac{\int_o^t z(mz+n)\left(E - \frac{(E-I)}{t}z\right)\mathrm{d}z}{\frac{A(E+I)}{2}} > 0 \tag{12}$$

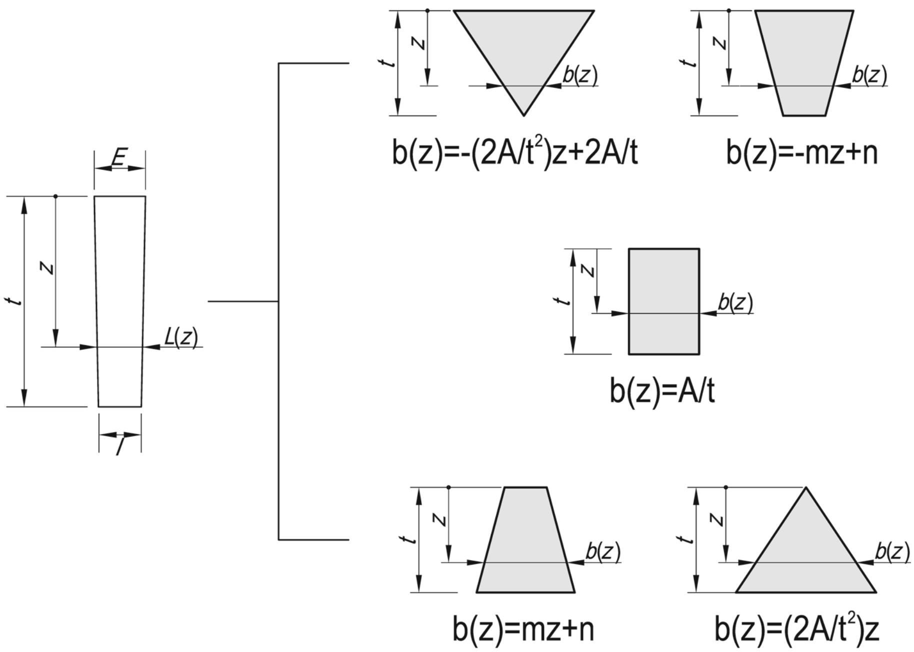

Fig. 6 On the left: geometrical parameters of the bi-dimensional voussoir. On the right: geometrical parameters of the normal cross-section considering a family of trapezoidal shapes according to $b(z) = mz + n$, with $-2A/t^2 \leq m \leq 2A/t^2$ and $0 \leq n \leq 2A/t$

Since A is always positive, it can be eliminated from both denominators and the expression can be simplified in Eq. (13). To demonstrate that $\eta = d_{E,S} - d_{E,V} > 0$, it is sufficient to demonstrate that the inequality of Eq. (13) holds.

$$\int_{o}^{t} z(mz+n)\mathrm{d}z - \frac{2}{E+I}\int_{o}^{t} z(mz+n)\left(E - \frac{E-I}{t}z\right)\mathrm{d}z > 0 \tag{13}$$

By expanding the second term of Eq. (13), Eq. (14) is obtained.

$$\frac{E-I}{E+I}\left(\frac{2}{t}\int_{o}^{t} z^2(mz+n)\mathrm{d}z - \int_{o}^{t} z(mz+n)\mathrm{d}z\right) > 0 \tag{14}$$

According to the geometric constraints of the voussoir, the term outside the parenthesis is always greater than 0, given that $E > I > 0$. Therefore, it is sufficient to demonstrate that the expression inside the parenthesis is positive, which leads to Eq. (15).

$$\int_{0}^{t}\left(\frac{2mz^3}{t} + \frac{2nz^2}{t} - mz^2 - nz\right)\mathrm{d}z > 0 \tag{15}$$

The integral is then resolved term by term, yielding the expression of Eq. (16).

$$\frac{2mt^3}{4} + \frac{2nt^2}{3} - \frac{mt^3}{3} - \frac{nt^2}{2} > 0 \tag{16}$$

Finally, the inequality is simplified in the expression of Eq. (17). Again, the geometric constraints of the voussoir are considered, namely, $t > 0$, and $b(z) = mz+n \geq 0$, with the exceptions of $b(z) = \frac{2A}{t^2}z$ and $b(z) = -\frac{2A}{t^2}z + \frac{2A}{t}$. Therefore, for $z = t$, $b(t) = mt+n > 0$. Thus, the inequality is demonstrated, and consequently it is also demonstrated that in any voussoir with a trapezoidal normal cross-section $\eta = d_{E,S} - d_{E,V} > 0$. This

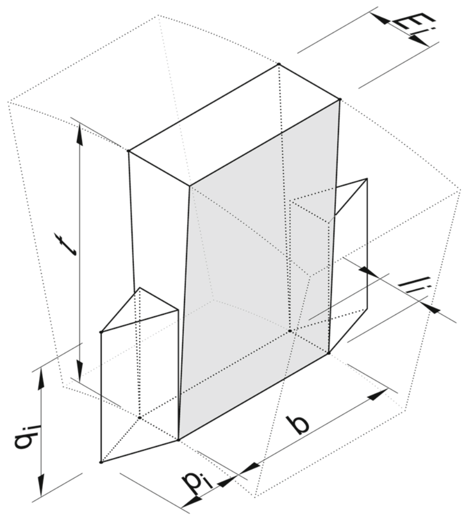

Fig. 7 Three-dimensional representation of the trapezoidal voussoir with the additional prisms on its lateral faces

in turn rules out the possibility of a continuous solution to the centroid eccentricity problem using trapezoidal voussoirs.

$$\frac{t^2}{6}(mt + n) > 0 \tag{17}$$

In the cases of $b(z) = \frac{2A}{t^2}z$ and $b(z) = -\frac{2A}{t^2}z + \frac{2A}{t}$, the family of trapezoidal cross-sections extends to include triangular cross-sections, corresponding to the limit cases $m = \pm 2A\big/t$. In these limit cases, we can calculate η by developing Eq. (10), that is, $\eta = t^2\big/(3(6R + t))$ and $\eta = t^2\big/(3(6R - t))$ respectively, which remains strictly positive, thus confirming that the impossibility of a continuous solution extends to triangular cross-sections as well. All of this motivates the search for discrete solutions, which are presented in Sect. 2.5.

2.5 Discrete solutions to the centroid eccentricity problem

2.5.1 Through additional prisms of variable dimensions affixed to the lateral faces of the voussoirs

Taking into account a normal rectangular cross-section, to position the centroids of the voussoirs on the catenary curve, it is necessary to move them towards the intrados of the arch, but without altering the position of the centroids of the normal sections. To achieve this, a volume is added to each voussoir in such a way that the shape of the delimiting normal sections is not altered. This additional volume is constituted by two right prisms, attached to the lateral faces of the voussoir. The base of each prism is a triangle coplanar with the intrados face of the voussoir. This triangular base is defined by p_i and I_i, and its height is defined by q_i, for each i^{th} voussoir, as illustrated in Fig. 7.

The volume V_i of the new voussoir is defined by Eq. (18). The eccentricity η_i of the voussoir's centroid with respect to the axis joining the centroids of the delimiting normal sections is defined by Eq. (19).

$$V_i = \frac{E_i + I_i}{2} tb + I_i p_i q_i \tag{18}$$

$$\eta_i = \frac{\frac{E_i+I_i}{2} tb\left(t - \frac{t(2I_i+E_i)}{3(I_i+E_i)}\right) + I_i p_i q_i \frac{q_i}{2}}{\frac{E_i+I_i}{2} tb + I_i p_i q_i} - \frac{t}{2} \tag{19}$$

If $\eta_i = 0$, both the centroidal axis and the axis joining the centroids of the normal sections coincide with the catenary curve, which defines the mid-axis line of the arch. Consequently, both axes coincide with the catenary curve which is located on the mid-axis line of the arch. Thus, a system of Eqs. (20–22) is obtained with which the design of each of the arch's voussoirs can be solved. Equation (20) results from the condition that $V_1 - V_i = 0$, and Eqs. (21) and (22) result from the conditions that $\eta_1 = 0$ and $\eta_i = 0$, respectively.

$$\frac{E_1 + I_1}{2} tb + I_1 p_1 q_1 - \frac{E_i + I_i}{2} tb - I_i p_i q_i = 0 \tag{20}$$

$$\frac{\frac{E_1+I_1}{2} tb\left(t - \frac{t(2I_1+E_1)}{3(I_1+E_1)}\right) + I_1 p_1 q_1 \frac{q_1}{2}}{\frac{E_1+I_1}{2} tb + I_1 p_1 q_1} - \frac{t}{2} = 0 \tag{21}$$

$$\frac{\frac{E_i+I_i}{2} tb\left(t - \frac{t(2I_i+E_i)}{3(I_i+E_i)}\right) + I_i p_i q_i \frac{q_i}{2}}{\frac{E_i+I_i}{2} tb + I_i p_i q_i} - \frac{t}{2} = 0 \tag{22}$$

$E_1, I_1, E_i and I_i$ with $i = 2 \div n$, p_1, t and b are known parameters. q_1 and p_i andq_i with $i = 2 \div n$ are unknown variables.

The unknown variables are isolated in Eqs. (23–25). To simplify, five auxiliary variables are introduced: ρ, *A, B, C* and *D*, defined in Eqs. (26–30).

$$q_1 = t\rho_{\pm} \tag{23}$$

$$q_i = \frac{1}{3} t \frac{-4bE_i - 2bI_i + 6I_1 p_1 \rho + 3b(E_1 + I_1)}{2I_1 p_1 \rho + b(E_1 + I_1 - E_i - I_i)} \tag{24}$$

$$p_i = \frac{1}{2I_i} \frac{A + B + C + D}{2b(-2E_i - I_i) + 6I_1 p_1 \rho + 3b(E_1 + I_1)} \tag{25}$$

$$\rho_{\pm} = \frac{1}{6I_1 p_1}\left(3I_1 p_1 \pm \sqrt{9I_1^2 p_1^2 - 6I_1 p_1 E_1 b + 6I_1^2 p_1 b}\right) \tag{26}$$

$$A = 12 p_1 \rho b I_1(-I_i + E_1 + I_1) \tag{27}$$

$$B = 12 p_1 \rho I_1(-bE_i + I_1 p_1) + 2bE_1 I_1(3b - p_1) \tag{28}$$

$$C = 2bI_1^2 p_1 + 3b^2\left(E_1^2 + I_1^2 + E_i^2 + I_i^2\right) \tag{29}$$

$$D = 6b^2(-E_1 E_i - E_1 I_i - I_1 E_i - I_1 I_i + E_i I_i) \tag{30}$$

Note that for any value of p_1, there are two distinct solutions for ρ in Eq. (26), depending on the sign of the root. Consequently, there are two solutions to the problem. However, there exists a value of p_1 such that $9I_1^2 p_1^2 - 6I_1 p_1 E_1 b + 6I_1^2 p_1 b = 0$, and consequently $\rho = 0.5$. By isolating p_1 in this expression, Eq. (31) is obtained. Thus, the minimum value of p_1 is established. This is due to the fact that below this value, Eq. (26) would have no solution. Therefore, it is assumed that $\rho = 0.5$ and consequently $p_1 = p_{1,\min}$.

$$p_{1,\min} = \frac{2b(E_1 - I_1)}{3I_1} \tag{31}$$

Figure 8 shows the elevation of six arches considering the same three catenary curves and the same two arch thicknesses t as for the six arches in Fig. 4, but with the addition of prisms on the lateral faces, allowing the centroidal axis (in red) to coincide with the catenary curve where the centroids of the delimiting normal sections are located. In this figure, the lines in the hatched area of each arch represent the prisms which are added to the side faces of the voussoirs to place their centroids on the catenary curve. These prisms are perpendicular to the catenary curve. The length of these lines corresponds to the dimension q_i of these additional prisms. It can be seen that this dimension increases from the keystone towards the arch's springing. This increment is more pronounced for arches with a higher H/L ratio.

Figure 9 illustrates how the dimensions of the additional prisms change across the length of the six arches shown in Fig. 8. Note that as the dimension q_i increases, the dimension p_i decreases; therefore the shape of the additional prisms varies along the arch, but all voussoirs have the same volume.

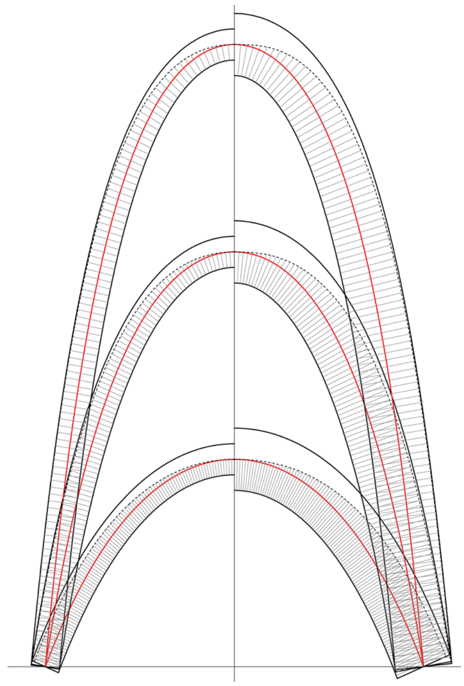

Fig. 8 Elevation of six arches considering the same three catenary curves and the same two arch thicknesses t used for the six arches in Fig. 4. The hatched area of each arch represents the additional prisms which are affixed to the sides of the voussoirs to place their centroids on the catenary curve

2.5.2 Through additional prisms of constant dimensions and variable position affixed to the lateral faces of the voussoirs

A second design can be considered in which the additional prisms have constant dimensions in all the voussoirs. These dimensions correspond to those of the keystone voussoir, i.e. I_1, p_1 and q_1, as determined in Eqs. (8), (23) and (31), respectively. Then, a new parameter, k_i, is defined as the distance between the intrados plane of the trapezoidal voussoir and the centroid of the additional prisms attached to the side faces. The value of this parameter for the keystone voussoir is $k_1 = q_1 \big/ 2$. The value of k_i varies across the length of the arch because the additional prisms are progressively displaced in the normal direction from the intrados to the extrados (Fig. 10).

The calculation of the value of k_i is achieved through Eq. (32). This equation is analogous to Eq. (22), incorporating the parameter k_i. Isolating this parameter, Eq. (33) is obtained, which can be used to calculate the value of k_i in the remaining voussoirs of the arch, considering $i = 2 \div n$.

$$\frac{\frac{E_i+I_i}{2} tb\left(t - \frac{t(2I_i+E_i)}{3(I_i+E_i)}\right) + I_1 pqk_i}{\frac{E_i+I_i}{2} tb + I_1 pq} - \frac{t}{2} = 0 \tag{32}$$

$$k_i = \frac{t}{2} - \frac{(E_i - I_i)bt^2}{12 I_1 pq} \tag{33}$$

Figure 11 illustrates the six arches from Figs. 4 and 8. In this case, the additional prisms on the side faces of the voussoirs are identical, but their position is adjusted in the normal direction to ensure that the centroid of each voussoir lies on the catenary curve. It is evident that the hatched area of each arch, where the additional prisms are located, is smaller than in the designs of Fig. 7. Proceeding along the entire length of the arch from the keystone to the springing, the additional prisms move from the intrados to a position almost centred on the catenary curve.

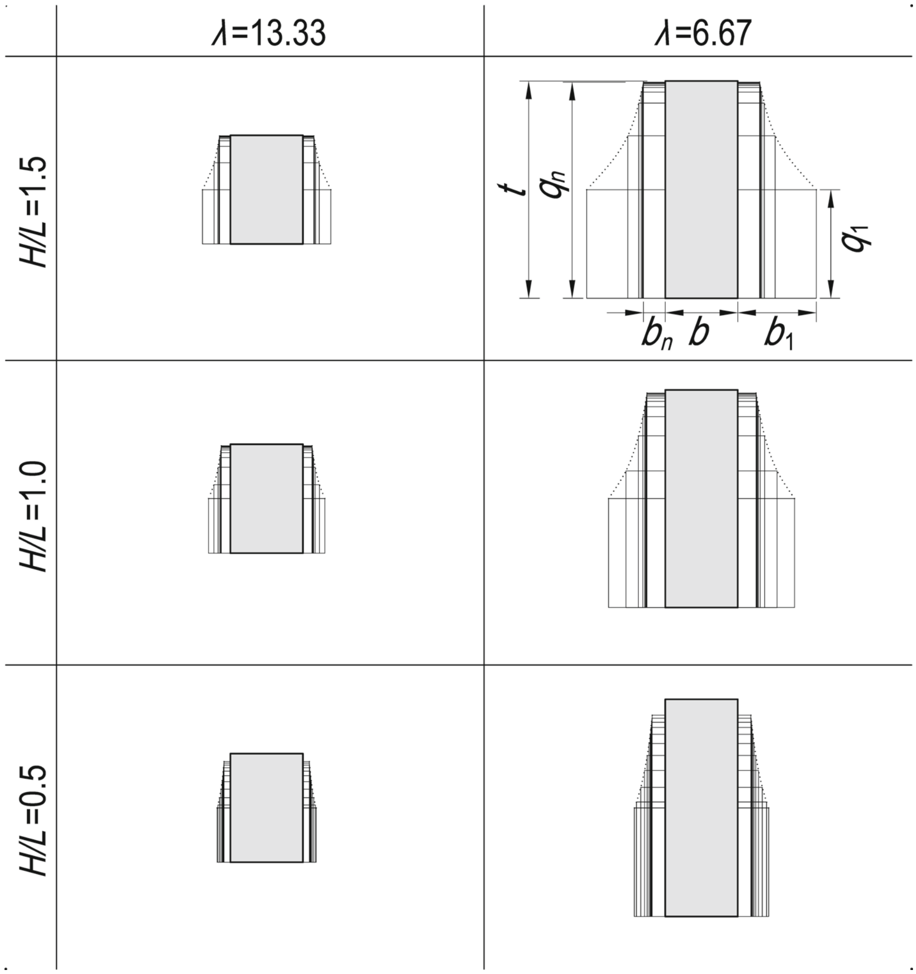

Fig. 9 Variation in the dimensions of the additional prisms across the length of the six arches in Fig. 8

2.5.3 Through additional prisms of variable dimensions affixed to the intrados and extrados faces of the voussoirs

The lateral prisms of the two previous designs prevent the composition of catenary vaults by extruding the arch profile along an axis perpendicular to the plane of the arch. For this reason, as an alternative to these two designs, a third design can be proposed. This third design considers two triangular prisms attached to the intrados and extrados faces of the voussoirs respectively. The position of the voussoir's centroid is controlled by varying the height p_i and q_i of the triangular prisms while keeping the volume constant (Fig. 12).

For the condition that $\eta_1 = 0$, Eq. (34) has been defined, analogous to Eq. (21). By means of calculations, the unknown dimension p_1, corresponding to the height of the triangular prism added on the intrados face of the keystone voussoir, was isolated in Eq. (35). In this voussoir, the volume of the intrados additional prism is maximum, and the volume of the extrados additional prism is zero.

$$\frac{\frac{E_1+I_1}{2}t\left(\frac{t(2I_1+E_1)}{3(I_1+E_1)}\right)+\frac{I_1p_1}{2}\left(t+\frac{p_1}{3}\right)}{\frac{E_1+I_1}{2}t+\frac{I_1p_1}{2}}-\frac{t}{2}=0 \tag{34}$$

$$p_1=\frac{t\left(\sqrt{I_1}\sqrt{I_1+8E_1}-3I_1\right)}{4I_1} \tag{35}$$

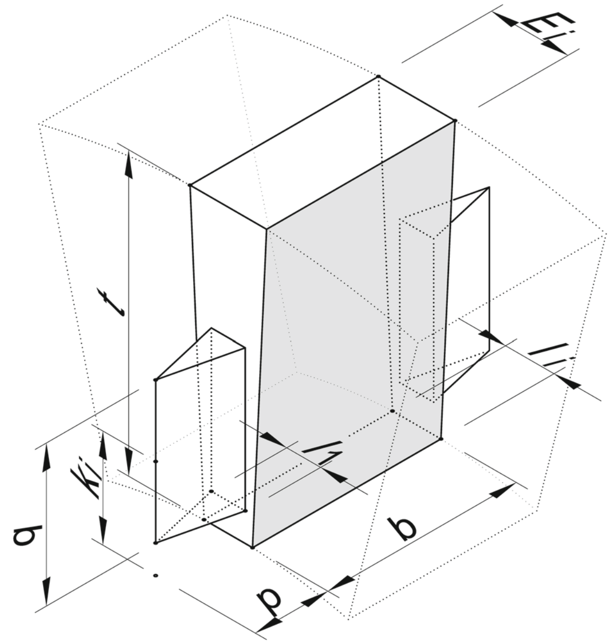

Fig. 10 Three-dimensional representation of the trapezoidal voussoir with additional prisms on the lateral faces. These prisms have constant dimensions and are displaced with respect to the plane of the intrados

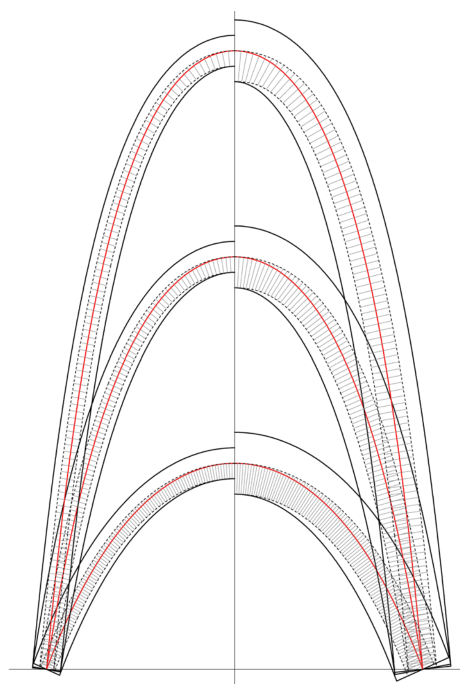

Fig. 11 Elevation of six arches considering the same three catenary curves and the same two distinct arch thicknesses t used in the six arches of Figs. 4 and 8. The hatched area represents the additional prisms attached to the lateral faces of the voussoirs

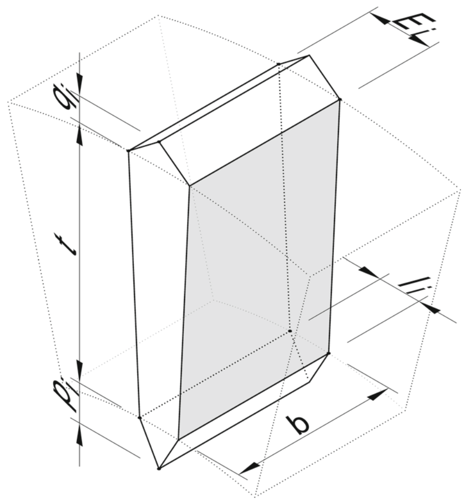

Fig. 12 Three-dimensional representation of the trapezoidal voussoir with additional triangular prisms on the intrados and extrados faces

Then, Eqs. (36) and (37) define the conditions that $V_1 - V_i = 0$ and $\eta_i = 0$ respectively. Again, by means of calculations, the unknown variables p_i and q_i are isolated in Eqs. (42) and (43). To simplify, some of their terms were replaced by four new variables: A, B, C and D. These new variables are defined in Eqs. (38–41).

$$\frac{I_1 p_1}{2} - \frac{E_i q_i}{2} - \frac{I_i p_i}{2} = 0 \tag{36}$$

$$\frac{\frac{E_i+I_i}{2} t \left(\frac{t(2I_i+E_i)}{3(I_i+E_i)} \right) + \frac{E_i q_i}{2} \left(-\frac{q_i}{3} \right) + \frac{I_i p_i}{2} \left(t + \frac{p_i}{3} \right)}{\frac{E_i+I_i}{2} t + \frac{E_i q_i}{2} + \frac{I_i p_i}{2}} - \frac{t}{2} = 0 \tag{37}$$

$$A = \frac{I_1 p_1}{2} \tag{38}$$

$$B = \frac{E_i + I_i}{2} t \tag{39}$$

$$C = \frac{t(2I_i + E_i)}{3(I_i + E_i)} \tag{40}$$

$$\begin{aligned} D = {} & 9I_i^2 E_i^2 t^2 + 12 I_i^2 E_i t A - 24 I_i E_i^2 BC + 16 I_i E_i A^2 + \\ & + 12 I_i E_i^2 t A + 12 I_i E_i^2 t B + 24 I_i^2 E_i BC - 12 I_i^2 E_i t B \end{aligned} \tag{41}$$

$$p_i = \frac{3 I_i E_i t + 4 A I_i - \sqrt{D}}{2\left(-I_i E_i + I_i^2\right)} \tag{42}$$

$$q_i = \frac{2}{E_i} \left(A - \frac{I_i p_i}{2} \right) \tag{43}$$

Figure 13 shows the same six arches represented in Figs. 4, 8 and 11. In this case, the additional prisms are located on the intrados and extrados faces of the voussoirs. Note that the height of the prisms on the intrados decreases from the top to the base of the arches, whereas the height of the prisms on the extrados increases from the top to the base. These additional prisms allow the centroid of each voussoir to be located on the catenary curve, coinciding with the mid-axis line of the arch and the centroids of the normal sections.

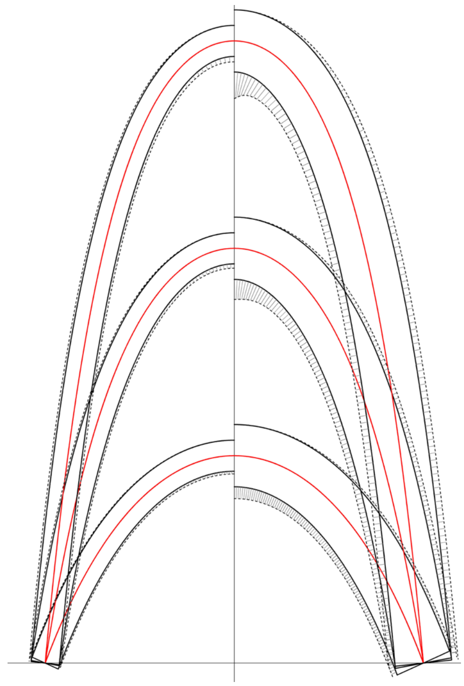

Fig. 13 Elevation of six arches considering the same three catenary curves and the same two distinct arch thicknesses t used in the six arches of Figs. 4, 8 and 11. The hatched area represents the additional prisms affixed to the extrados and intrados faces of the voussoirs

3 Results and discussion

The ratio σ_M / σ_N calculated in subSect. 2.3 expressed, in fact, the increase of the normal stresses σ_M due to the bending moment at the keystone with respect to the normal stress considering only the axial force. Similarly, a ratio $\sigma_{N,ad} / \sigma_N$ can be calculated to express the increase of the normal stress $\sigma_{N,ad}$ due to the increase of the axial force caused by the weight of the additional prisms with respect to the normal stress σ_N of the same arch without the additional prisms. These ratios have been represented in two graphics analogous to that in Fig. 5b (Figs. 14a, b), for two locations of the additional prisms: lateral faces (a), and intrados and extrados faces (b). As anticipated in subSect. 2.3, this comparison allows one to demonstrate that the structural penalty introduced by the additional prisms in arches geometrically compatible with a bending-moment-free state is smaller than the structural penalty due to the bending moment in the optimal state of a conventional catenary arch.

A comparison of the three graphics (Figs. 5b, 14a, b) shows the following:

- The increase in the normal stress due to the bending moment (Fig. 5b) is greater than due to the weight of the additional prisms in the catenary arches geometrically compatible with a bending-moment-free state (Figs. 14a, b).
- The increase in the normal stress due to the weight of the additional prisms located on the lateral faces of the voussoirs is greater than the same increase when the additional prisms are located on the intrados and extrados faces.

As mentioned in subSects. 1.3 and 2.2, the accuracy of the solution increases with the number n of voussoirs. To quantify this accuracy, catenary arch with additional prisms on the intrados and extrados of the voussoirs is considered (Fig. 15a, b). We define the distance δ_1 between the catenary curve and the polygonal axis joining the centroids of the normal sections (in blue color in Fig. 15c), and the distance δ_2 between the catenary curve and polygonal axis joining the centroids of the voussoirs (in red color in Fig. 15c). Furthermore, we considered the eccentricity η between the catenary curve and the original centroidal axis (in red dot line in Fig. 15c).

If $n >> 1$, any local group of adjacent voussoirs subtends a sufficiently small arc of the catenary curve that R can be considered uniform among them (Fig. 15c). Then, the distance δ_1 from the catenary curve to the polygonal axis joining the centroids of the normal cross-sections (in blue) can be calculated with Eq. (44) as the difference between the radius of curvature R and the distance between the center of curvature and the

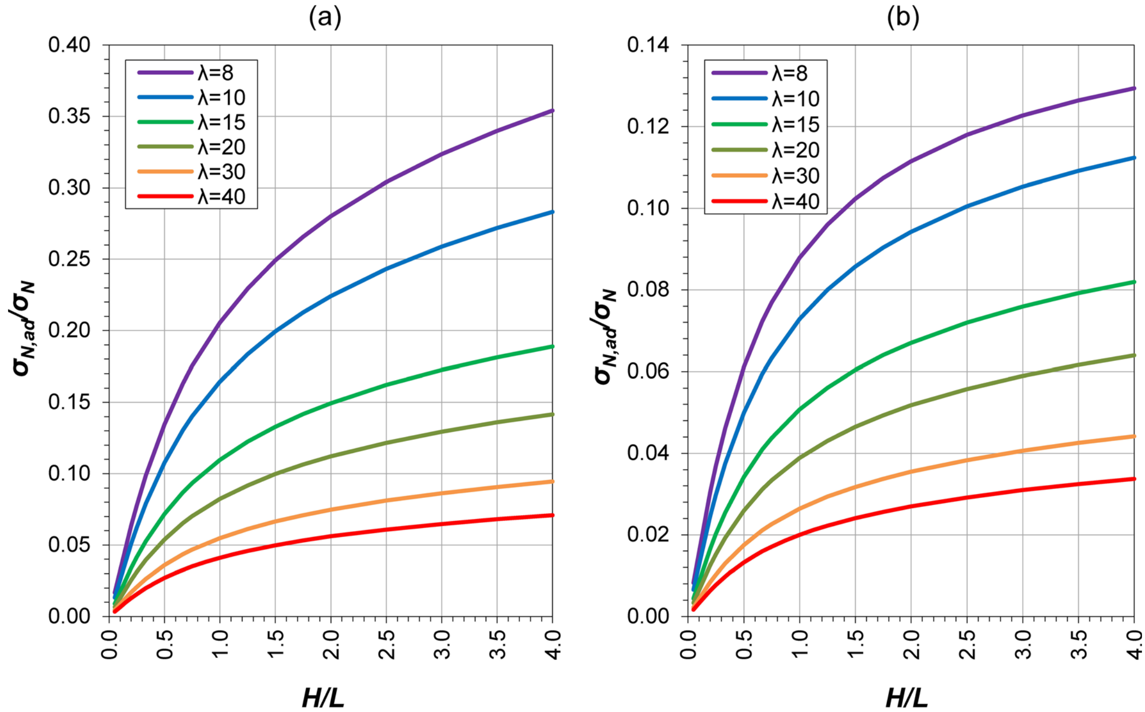

Fig. 14 Ratio $\sigma_{N,ad}/\sigma_N$ for six distinct slendernesses $\lambda = L/t$, depending on arch's H/L ratio and on the location of the additional prisms: lateral faces (**a**); intrados and extrados faces (**b**)

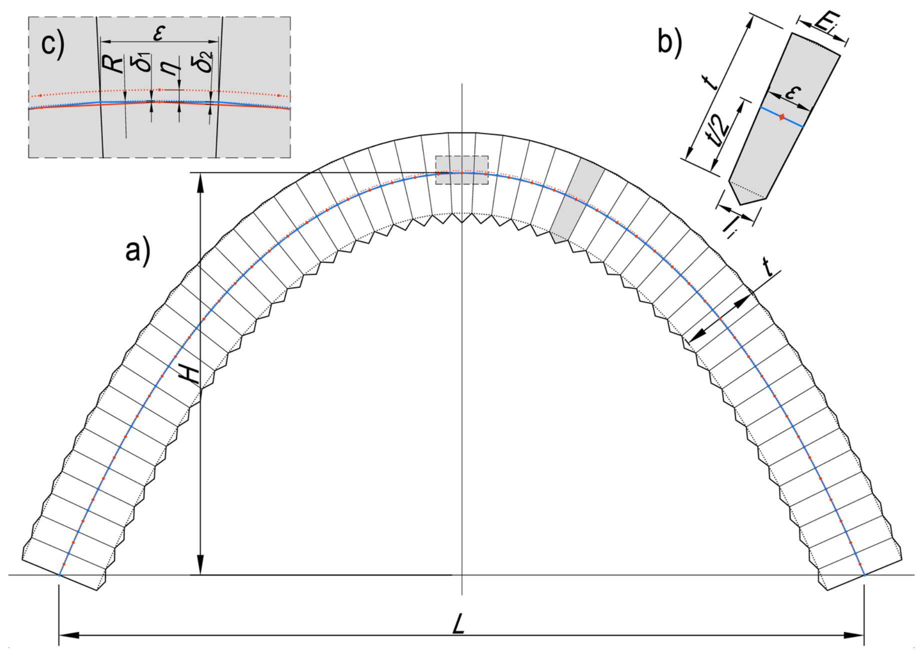

Fig. 15 Catenary arch with additional prisms on the intrados and extrados of the voussoirs (**a**); parameters of the voussoirs (**b**); parameters for the accuracy quantification in a local group of voussoirs (**c**)

midpoint of the side of this first polygonal axis, i.e., ε, with $\varepsilon = s/n$ where n is the number of voussoirs and s is the total length s of the catenary curve calculated by Eq. (5).

$$\delta_1 = R - \sqrt{R^2 - \left(\frac{s}{2n}\right)^2} \tag{44}$$

Similarly, the distance δ_2 from the catenary curve to the polygonal axis joining the centroids of the voussoirs (in red) can be calculated as the difference between the radius of curvature R and the distance between the center of curvature and the midpoint of the side of this second polygonal axis, which length is not $\varepsilon = s/n$, but $s\sqrt{R^2 - \left(\frac{s}{2n}\right)^2} \Big/ nR$.This has been expressed in Eq. (45).

$$\delta_2 = R - \sqrt{R^2 - \left(\frac{s}{2n}\right)^2 - \left(R^2 - \left(\frac{s}{2n}\right)^2\right)\left(\frac{s}{2nR}\right)^2} \tag{45}$$

The Eq. (45) has been simplified in Eq. (46) by factoring $\left(R^2 - \left(\frac{s}{2n}\right)^2\right)$ inside the root.

$$\delta_2 = R - \sqrt{\left(R^2 - \left(\frac{s}{2n}\right)^2\right)\left(1 - \left(\frac{s}{2nR}\right)^2\right)} \tag{46}$$

Since $\delta_2 > \delta_1$, the condition for the minimum accuracy can be defined as $\delta_2 \leq \eta$. This criterion ensures that deviation δ_2 in the location of the voussoir centroids is smaller than the eccentricity η that the method intends to correct. Then, in Eq. (47) have been equated Eq. (1) and Eq. (46).

$$\frac{t^2}{12R} = R - \sqrt{\left(R^2 - \left(\frac{s}{2n}\right)^2\right)\left(1 - \left(\frac{s}{2nR}\right)^2\right)} \tag{47}$$

Finally, n has been isolated in Eq. (48), finding its minimum value, that is, $n_{\min}$.

$$n_{\min} = \frac{s\sqrt{3}}{t} \tag{48}$$

Considering the arch in Fig. 15a, with $L = 20$ m, $H = 20$ m, and $t = 2$ m, $n = 51$, and consequently $\varepsilon = 0.587$ m, the resulting minimum number of voussoirs is $n_{\min} = 26$, and consequently, the maximum length of the voussoirs is $\varepsilon_{\max} = 1.151$ m. That is, in this case, the accuracy of the discrete method with $n = 51$ is clearly sufficient. Indeed, since δ_2 scales approximately with $1\big/n^2$ 1/n^2, a number of voussoirs only about twice $n_{\min}$ already reduces δ_2 to approximately η/4, well below the minimum accuracy threshold.

In Fig. 16, graphic statics has been used to verify that a thrust line (in red) exists that, with sufficient precision guaranteed by $n >> n_{\min}$, is indistinguishable from the axis joining centroids of the normal cross-sections of the arch (in blue) of the previous example, describing a catenary curve. To this end, the loads have been applied at the real volumetric centroids (in red) of the voussoirs, which, thanks to the proposed method, are aligned with the centroids of the normal cross-sections and therefore with the catenary, with the same precision. This demonstrates that the arch designed using the proposed method is geometrically compatible with a bending-moment-free state, thus validating the design obtained through the closed-form expressions defined in Sect. 2. Within the adopted framework, the existence of a single admissible thrust line coinciding with the catenary axis is sufficient to establish that the arch is geometrically compatible with a bending-moment-free state, regardless of which equilibrium state is actually realized.

Recent studies have explored form-finding, parametric design and 3D printing techniques in an integrated design-to-fabrication process of arches and vaulted structures [42–45]. The use of 3D printing techniques in the manufacture of the voussoirs would allow the additional prisms to be precisely reproduced as surface reliefs on each voussoir. The size of the virtual voussoirs must be kept small to ensure high precision. However, in 3D printing, each manufactured voussoir could contain several virtual voussoirs. Thus, it would be possible to adjust the size of the virtual voussoirs, and therefore of the additional prisms, to ensure high design precision while remaining within the precision limits of the 3D printing technique.

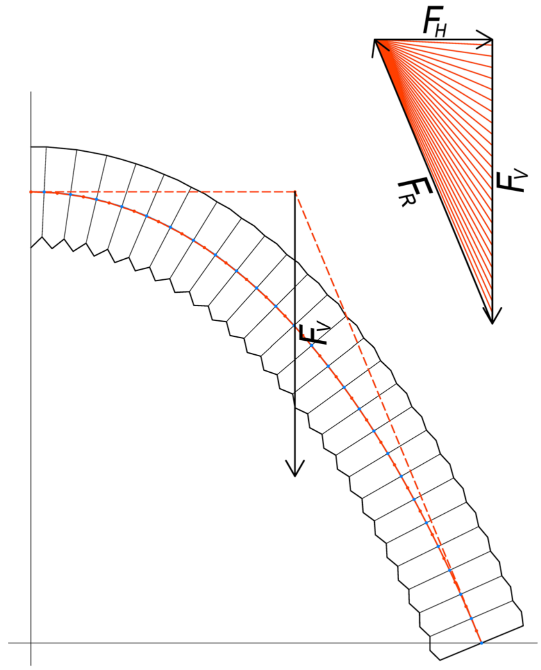

Fig. 16 Semi-catenary arch designed using the proposed method, with additional prisms on the intrados and extrados faces of the voussoirs. The thrust line (in red) is verified by graphic statics to be indistinguishable from the axis joining the centroids of the normal cross-sections (in blue), demonstrating that the arch is geometrically compatible with a bending-moment-free state

4 Conclusions

This paper has addressed the paradox of the bending-moment-free catenary arch, which can be stated as follows: although a one-dimensional catenary arch subjected to its self-weight is simply compressed and bending-moment-free, when this arch is three-dimensional and has a constant rectangular cross-section of finite dimensions, the centroids of its voussoirs are not located on the catenary curve where the centroids of its normal sections are located, but are displaced towards the extrados of the arch. This displacement, therefore, prevents the arch from being geometrically compatible with a bending-moment-free state. Furthermore, it is demonstrated that the impossibility of achieving a bending-moment-free state is not exclusive to voussoirs with a rectangular normal cross-section, but extends to any voussoir with trapezoidal cross section. For any function $b(z) = mz+n > 0$ with $z = 0 \div t$, the distance η between the centroid of the voussoir and the centroid of the normal section is strictly positive, which rules out any continuous solution to the centroid eccentricity problem.

Since the impossibility of a continuous solution extends to the entire family of trapezoidal cross-sections, as a solution to this paradox, this paper presents a method for designing a three-dimensional arch whose centroidal axis coincides with the catenary curve resulting from joining the centroids of the arch's normal sections. This ensures that the catenary arch is geometrically compatible with a simply compressed, bending-moment-free state. The proposed method is based on the discretisation of the arch into small trapezoidal prismatic voussoirs of constant rectangular cross-section. Initially, an eccentricity exists between the axis joining the centroids of the voussoirs and the axis joining the centroids of the normal sections. However, by adding prismatic volumes to the lateral surfaces of each voussoir, the centroid of each voussoir can be repositioned onto the catenary curve without altering the shape or position of the centroids of the normal sections. Three alternative designs for the voussoir geometry have been developed and analysed. In addition, application examples have been presented taking into account different catenary curves. Based on these examples, graphs have been produced to illustrate how the shape of the voussoirs changes across the length of the arch. Furthermore, a closed-form expression for the minimum number of voussoirs is derived, which ensures that the deviation in the location of the voussoir centroids is smaller than the eccentricity η that the method aims to correct. A representative example is presented in which the method is applied using a number of voussoirs $n >> n_{\min}$, confirming that the precision of the discrete method is more than sufficient for practical purposes. Finally, the design obtained is verified by graphic statics, confirming that a thrust line passing through the centroids of the normal cross-sections exists, and thus that the arch designed using the proposed method is geometrically compatible with a bending-moment-free state. Future work could explore the application of this discrete method to other funicular arches with different load distribution patterns, such as those used in deck-arch bridges [46, 47].

This method is expected to contribute to the improvement of the design of funicular arches, by correcting the eccentricity between the centroidal axis and the axis joining the centroids of the normal cross-sections. The problem is formulated as a geometric optimization of the voussoir shape, offering a closed-form analytical solution that avoids the need for iterative numerical optimization algorithms. The demonstration of the impossibility of a continuous solution for both rectangular and trapezoidal cross-sections reinforces the relevance of this discrete approach as a viable means of solving the problem.

Author contributions R. Martín-Sáiz: conceptualization, analysis, writing, formal modeling and final review; and B. Herrera: analysis, supervision and review. All authors approved the final manuscript.

Funding Open Access funding provided thanks to the CRUE-CSIC agreement with Springer Nature. No funding was received for conducting this study.

Data availability The datasets generated during the current study are available from the corresponding author on reasonable request. All results presented in the figures can be reproduced by applying the analytical expressions provided in Sect. 2.

Declarations

Conflict of interest The authors declare no competing interests.

Replication of results The results presented in this paper can be replicated by applying the closed-form analytical expressions derived in Sect. 2. The geometry of the arch and each voussoir is fully determined by Eqs. (1–48), which require only two input parameters: the span L and the height H of the arch. The catenary curve parameters a and c are obtained by solving the system formed by Eqs. (2) and (3) using the Newton–Raphson method. The eccentricity of each voussoir's centroid, the dimensions of the additional prisms and the minimum number of voussoirs are subsequently calculated through the explicit expressions provided in Eqs. (18–48), without the need for iterative numerical methods. No external code or dataset is required to reproduce the figures and results shown in this paper, as all numerical values can be derived directly from the equations presented herein.

References

1. Nikolić, D.: A note on the catenary arch bending-moment-free paradox. Meccanica **57**(6), 457–462 (2022). https://doi.org/10.1007/s11012-022-01513-9
2. Hooke, R.: A Description of Helioscopes, and Some Other Instruments. Royal Society, London (1675)
3. Leibniz, G.W.: De linea in quam flexible se pondere curvat. Acta Eruditorum June, 277–291 (1691)
4. Huygens, C:. Dynastae Zulichemii, solutio problematis funicularii. Acta Eruditorum June, 281–282 (1691)
5. Bernoulli, J.O.: Solutio problematis funicularii. Acta Eruditorum June, 274–276 (1691)
6. Bernoulli, J.A.: Analysis problematis ante hac propositi, de inventione lineae descensus. Acta Eruditorum May, 217–219 (1690)
7. Gregory, D.: Catenaria. Philos. Trans. Royal Soc. **19** (231), 637–652 (1697). https://doi.org/10.1098/rstl.1695.0114
8. Stirling, J.: Methodus disponendi quotcunque sphæras in fornicem. Et inde demonstratur propietas præcipua curvæ catenariæ. In Lineæ tertii ordinis Neutonianæ, Oxford (1717).
9. Poleni, G.: Memorie istoriche della gran cupola del Tempio Vaticano. Padova (1748)
10. Heyman, J.: The Stone Skeleton: Structural Engineering of Masonry Architecture. Cambridge University Press, Cambridge (1995)
11. Graefe, R.: The catenary and the line of thrust as a means for shaping arches and vaults. In: Physical Models: Their Historical and Current Use in Civil and Building Engineering Design, pp. 79–126. John Wiley & Sons, Berlin (2020)
12. Makris, N., Alexakis, H.: The effect of stereotomy on the shape of the thrust-line and the minimum thickness of semicircular masonry arches. Arch. Appl. Mech. **83**, 1511–1533 (2013). https://doi.org/10.1007/s00419-013-0763-4
13. Alexakis, H., Makris, N.: Minimum thickness of elliptical masonry arches. Acta Mech. **224**, 2977–2991 (2013). https://doi.org/10.1007/s00707-013-0906-2

14. Alexakis, H., Makris, N.: Limit equilibrium analysis of masonry arches. Arch. Appl. Mech. **85**(9), 1363–1381 (2015). https://doi.org/10.1007/s00419-014-0963-6
15. Gaspar, O., Sajtos, I.: On the definition of the line of thrust. In: Van Balen, K., Verstrynge, E. (eds.) Structural Analysis of Historical Constructions: Anamnesis, Diagnosis, Therapy, Controls, pp. 1003–1010. CRC Press, Leiden (2016)
16. Marano, G.C., Trentadue, F., Petrone, F.: Optimal arch shape solution under static vertical loads. Acta Mech. **225**, 679–686 (2014). https://doi.org/10.1007/s00707-013-0985-0
17. Wang, C.Y., Wang, C.M.: Closed-form solutions for funicular cables and arches. Acta Mech. **226**, 1641–1645 (2015). https://doi.org/10.1007/s00707-014-1250-x
18. Lewis, W.J.: Mathematical model of a moment-less arch. Proc. R. Soc. A **472**(2190), 20160019 (2016). https://doi.org/10.1098/rspa.2016.0019
19. Salimbeni, L.: Degli archi e delle volte. Dionigi Ramanzini, Verona (1787)
20. Milanković, M.: Theorie der Druckkurven. Zeitschrift für Mathematik und Physik **55**, 1–27 (1907)
21. Foce, F.: Milankovitch's Theorie der Druckkurven: good mechanics for masonry architecture. Nexus Netw. J. **9**, 185–210 (2007). https://doi.org/10.1007/s00004-007-0039-9
22. Nikolić, D.: Catenary arch of finite thickness as the optimal arch shape. Struct. Multidiscip. Optim. **60**(5), 1957–1966 (2019). https://doi.org/10.1007/s00158-019-02304-9
23. Nodargi, N.A., Bisegna, P.: Thrust line analysis revisited and applied to optimization of masonry arches. Int. J. Mech. Sci. **79**, 105690 (2020). https://doi.org/10.1016/j.ijmecsci.2020.105690
24. Nodargi, N.A., Bisegna, P.: A unifying computational approach for the lower-bound limit analysis of systems of masonry arches and buttresses. Eng. Struct. **221**, 110999 (2020). https://doi.org/10.1016/j.engstruct.2020.110999
25. Alexakis, H., Makris, N.: Vector analysis and the stationary potential energy for assessing equilibrium of curved masonry structures. Math. Mech. Solids **30**(1), 40–56 (2025). https://doi.org/10.1177/10812865231118335
26. Kooharian, A.: Limit analysis of voussoir (segmental) and concrete arches. ACI J. Proc. **49**(12), 317–328 (1952)
27. Heyman, J.: The stone skeleton. Int. J. Solids Struct. **2**(2), 249–279 (1966). https://doi.org/10.1016/0020-7683(66)90018-7
28. Heyman, J.: The safety of masonry arches. Int. J. Mech. Sci. **11**(4), 363–385 (1969). https://doi.org/10.1016/0020-7403(69)90070-8
29. Sinopoli, A., Corradi, M., Foce, F.: Modern formulation for preelastic theories on masonry arches. J. Eng. Mech. **123**(3), 204–213 (1997). https://doi.org/10.1061/(ASCE)0733-9399(1997)123:3(204
30. Huerta, S.: Mechanics of masonry vaults: the equilibrium approach. In: Structural Analysis of Historical Constructions, pp. 47–69. RILEM Publications (2001)
31. Ochsendorf, J.A.: Collapse of masonry structures. PhD Thesis, University of Cambridge, Cambridge, UK (2002).
32. Andreu, A., Gil, L., Roca, P.: Computational analysis of masonry structures with a funicular model. J. Eng. Mech. **133**(4), 473–480 (2007). https://doi.org/10.1061/(ASCE)0733-9399(2007)133:4(473)
33. Marmo, F.: ArchLab: a MATLAB tool for the thrust line analysis of masonry arches. Curv. Layer. Struct. (2021). https://doi.org/10.1515/cls-2021-0003
34. Nanayakkara, K.I.U., Liew, A., Gilbert, M.: Application of thrust layout optimization to masonry structures. Proc. Royal Soc. A Math. Phys. Eng. Sci. **479**(2273), 20230053 (2023). https://doi.org/10.1098/rspa.2023.0053
35. Block, P., DeJong, M., Ochsendorf, J.: As hangs the flexible line: equilibrium of masonry arches. Nexus Netw. J. **8**(2), 13–24 (2006)
36. Block, P., Ciblac, T., Ochsendorf, J.: Real-time limit analysis of vaulted masonry buildings. Comput. Struct. **84**(29–30), 1841–1852 (2006). https://doi.org/10.1016/j.compstruc.2006.08.002
37. Block, P., Ochsendorf, J.: Thrust network analysis: a new methodology for three-dimensional equilibrium. J. Int. Assoc. Shell Spat. Struct. **48**(3), 167–173 (2007)
38. Rippmann, M., Lachauer, L., Block, P.: Interactive vault design. Int. J. Space Struct. **27**(4), 219–230 (2012). https://doi.org/10.1260/0266-3511.27.4.219
39. Tempesta, G., Galassi, S.: Safety evaluation of masonry arches. A numerical procedure based on the thrust line closest to the geometrical axis. Int. J. Mech. Sci. **155**, 206–221 (2019). https://doi.org/10.1016/j.ijmecsci.2019.02.036
40. Galassi, S., Tempesta, G.: The Matlab code of the method based on the full range factor for assessing the safety of masonry arches. MethodsX **6**, 1521–1542 (2019). https://doi.org/10.1016/j.mex.2019.05.033
41. Galassi, S., Tempesta, G.: Safety assessment of masonry undamaged and damaged arches subjected to gravitational loads and horizontal forces. A numeric procedure to identify the optimal thrust line. Int. J. Solids Struct. **301**, 112943 (2024). https://doi.org/10.1016/j.ijsolstr.2024.112943
42. Rippmann, M.: Funicular shell design: geometric approaches to form finding and fabrication of discrete funicular structures. PhD Thesis Dissertation, ETH Zurich (2016).
43. Riberi, F.: Form finding and optimal brick tessellation for static equilibrium of a pierced vault. PhD Thesis Dissertation, Politecnico di Torino (2018)
44. Bhooshan, S., Bhooshan, V., Dell'Endice, A., et al.: The Striatus bridge: computational design and robotic fabrication of an unreinforced, 3D-concrete-printed, masonry arch bridge. Arch. Struct. Constr. **2**(4), 521–543 (2022). https://doi.org/10.1007/s44150-022-00051-y
45. Dell'Endice, A., Bouten, S., Van Mele, T., Block, P.: Structural design and engineering of Striatus, an unreinforced 3D-concrete-printed masonry arch bridge. Eng. Struct. **292**, 116534 (2023). https://doi.org/10.1016/j.engstruct.2023.116534
46. Trentadue, F., Marano, G.C., Vanzi, I., Briseghella, B.: Optimal arches shape for single-point-supported deck bridges. Acta Mech. **229**, 2291–2297 (2018). https://doi.org/10.1007/s00707-017-2084-0
47. Zhang, G., Liu, Y., Zhao, W., Liu, Z., Liu, J., Feng, B.: Optimal arch shape of long-span open-spandrel arch bridges under vertical permanent loads. Structures **45**, 1012–1030 (2022). https://doi.org/10.1016/j.istruc.2022.09.086